Disruption of the exocyst induces podocyte loss and dysfunction

Received for publication, March 8, 2019, and in revised form, May 6, 2019 Published, Papers in Press, May 9, 2019, DOI 10.1074/jbc.RA119.008362

Deepak Nihalani[‡1,2], Ashish K. Solanki[‡1], Ehtesham Arif[‡], Pankaj Srivastava[‡], Bushra Rahman[‡], Xiaofeng Zuo[‡], Yujing Dang[‡], Ben Fogelgren[§], Damian Fermin[¶], Christopher E. Gillies[¶], Matthew G. Sampson[¶‖], and Joshua H. Lipschutz[‡1]**

*From the [‡]Department of Medicine, Medical University of South Carolina, Charleston, South Carolina 29425, the [§]Department of Anatomy, Biochemistry, and Physiology, University of Hawaii at Manoa, Honolulu, Hawaii 96813, the [¶]Department of Pediatrics–Nephrology and [‖]Center for Computational Medicine and Bioinformatics, University of Michigan, Ann Arbor, Michigan 48109, and the **Department of Medicine, Ralph H. Johnson Veterans Affairs Medical Center, Charleston, South Carolina 29401*

Edited by Peter Cresswell

Although the slit diaphragm proteins in podocytes are uniquely organized to maintain glomerular filtration assembly and function, little is known about the underlying mechanisms that participate in trafficking these proteins to the correct location for development and homeostasis. Identifying these mechanisms will likely provide novel targets for therapeutic intervention to preserve podocyte function following glomerular injury. Analysis of structural variation in cases of human nephrotic syndrome identified rare heterozygous deletions of *EXOC4* in two patients. This suggested that disruption of the highly-conserved eight-protein exocyst trafficking complex could have a role in podocyte dysfunction. Indeed, mRNA profiling of injured podocytes identified significant exocyst down-regulation. To test the hypothesis that the exocyst is centrally involved in podocyte development/function, we generated homozygous podocyte-specific Exoc5 (a central exocyst component that interacts with Exoc4) knockout mice that showed massive proteinuria and died within 4 weeks of birth. Histological and ultrastructural analysis of these mice showed severe glomerular defects with increased fibrosis, proteinaceous casts, effaced podocytes, and loss of the slit diaphragm. Immunofluorescence analysis revealed that Neph1 and Nephrin, major slit diaphragm constituents, were mislocalized and/or lost. mRNA profiling of Exoc5 knockdown podocytes showed that vesicular trafficking was the most affected cellular event. Mapping of signaling pathways and Western blot analysis revealed significant up-regulation of the mitogen-activated protein kinase and transforming growth factor-β pathways in Exoc5 knockdown podocytes and in the glomeruli of podocyte-specific Exoc5 KO mice. Based on these data, we propose that exocyst-based mechanisms regulate Neph1 and Nephrin signaling and trafficking, and thus podocyte development and function.

Diseases that cause podocyte dysfunction and loss are the leading causes of end-stage kidney disease worldwide. Targeting the early molecular events in podocyte development and/or homeostasis may lead to an effective therapy to manage podocyte injury and recovery, which is critical given the paucity, and toxicity, of current therapies. The slit diaphragm proteins Nephrin and Neph1 are known to regulate podocyte actin dynamics through their ability to assemble a signaling cascade that leads to structural and functional changes in podocytes (1–3). The membrane organization of Nephrin and Neph1 is critical for cell survival, and several recent reports highlight changes in their localization, where they are displaced from the slit diaphragm, in response to glomerular injury (2–5). Reports have also emerged that demonstrate endocytic trafficking of these proteins as a critical event in podocyte function (6).

The exocyst is a highly-conserved octameric protein complex composed of Exoc1–8 that mediates the targeting and docking of vesicles carrying membrane proteins (7). Various cellular processes have been shown by us and others that involve the exocyst, including cell polarity (8, 9), ciliogenesis (10–13), and protein translation (14, 15). Although the exocyst complex is a hetero-octameric protein complex, Exoc5 is a central component of the exocyst (9, 13), loss of which leads to disintegration of this complex (13, 16). Exocyst complex members were also shown to be mutated in families with diseases that can affect the kidney, such as Joubert syndrome (17); however, the role of the exocyst complex in podocyte biology has not been investigated.

Our recent results identified two patients with exocyst 4 (EXOC4) deletions from a cohort of 256 patients with nephrotic syndrome, which prompted us to further investigate the role of the exocyst complex in podocytes by generating podocyte-specific Exoc5 knockout (KO) mice. In this study, we demonstrate the phenotypic and mechanistic analyses of these mice, which show that loss of Exoc5 induced podocyte cell death and proteinuria. We

This work was supported in part by Veterans Affairs Merit Award I01 BX000820 (to J. H. L.), National Institutes of Health Grants P30DK074038 (to J. H. L.), R01DK087956 (to D. N.), and RO1DK108805 (to M. G. S.), South Carolina SmartState Centers of Excellence Endowment (to D. N.), SCTR NIH/NCATS Grant 5UL1TR001450 (to D. N. and E. A.), the American Heart Association AWRP Winter 2017 Collaborative Sciences Award (to J. H. L.), the Ben J. Lipps Research Fellowship from the American Society of Nephrology (to A. K. S.), the Charles Woodson Clinical Research Fund (to M. G. S.), and the Ravitz Foundation (to M. G. S.). The authors declare that they have no conflicts of interest with the contents of this article. The content is solely the responsibility of the authors and does not necessarily represent the official views of the National Institutes of Health.

This article contains Figs. S1–S4.

[1] These authors contributed equally to this work.

[2] To whom correspondence should be addressed: SmartState Renal Biomarkers Chair, Medical University of South Carolina, 96 Jonathan Lucas St., CSB 829, Charleston, SC 29425. Tel.: 843-792-7659; Fax: 843-792-8399; E-mail: nihalani@musc.edu.

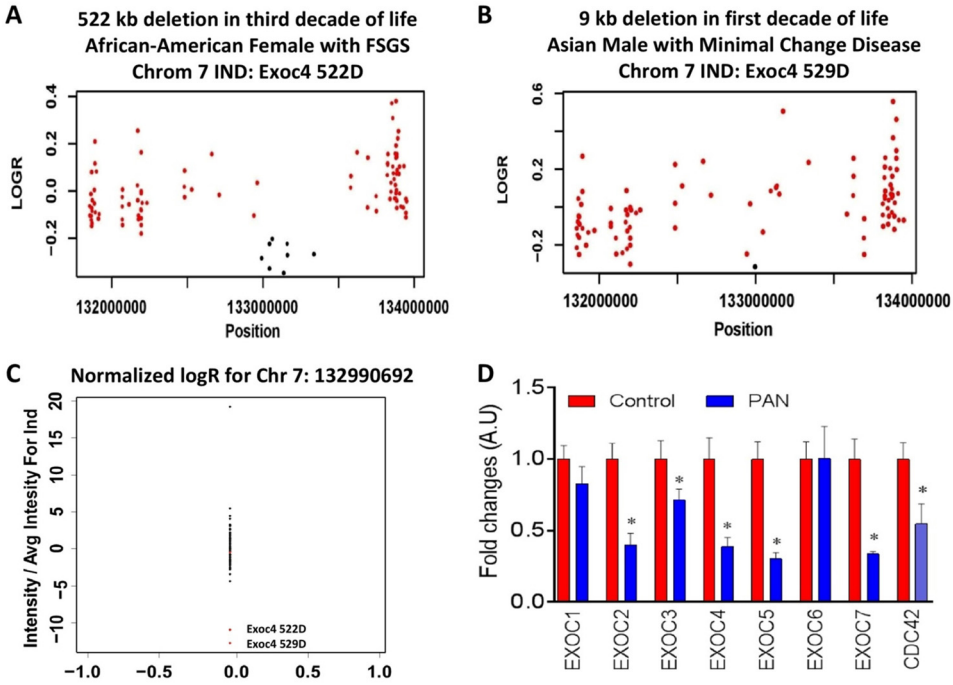

Figure 1. Intensities of the CNV region using exome chip genotypes acquired from the patients. *A–C,* log *R* ratio from exome chip data at the Chr. 7: locus is presented. *Black dots,* SNPs within the CNV region. Smaller values on *y* axis, lower intensity is supportive of a deletion. *D,* expression level of exocyst complex members decreases following injury with PAN. mRNA profiling of podocytes injured with PAN showed down-regulation of various components of the exocyst complex and its regulator CDC42. (*, $p < 0.05$, paired Student's *t* test).

further demonstrate that mislocalization of Nephrin and Neph1 is a major contributor to this phenotype.

Results

Identification of structural variation revealed deletions in the exons of EXOC4, a member of the exocyst complex, in two patients with nephrotic syndrome

Structural variation (SV)[3] represents a form of genomic variation that can cause or be associated with human disease (18), and it is known to impact between 15 and 20% of all children born with abnormally developed kidneys (19). Therefore, SV analysis was performed on 256 patients with nephrotic syndrome enrolled in the Nephrotic Syndrome Study Network (NEPTUNE) (20), who had undergone whole-genome sequencing and Illumina ExomeArray Genotyping. By doing this, we identified two patients with heterozygous deletions on chromosome 17 impacting *EXOC4*. EXOC4 is an exocyst component that directly interacts with EXOC5 (21, 22). One patient had a 522-kb deletion (Chr. 17: 132,970,005–133,492,495, deleting exons 3–10), and the other had a 9-kb deletion (Chr. 17: 132,987,872–132,997,017 deleting exon 3) in the *EXOC4* gene (Fig. 1, *A* and *B*, *black dots* represent SNPs within the copy-number variation (CNV) region and have a lower log *R* ratio). These heterozygous deletions were independently validated by mapping the intensity of the signals for these SNPs in the entire cohort, identifying the two cases with deletions as having the lowest intensity (Fig. 1*C*). In the 2,504 member "1000 Genomes Project cohort," there was only one individual with an SV overlapping the *EXOC4*-coding sequence, and this affected only exon 15. Although both patients had nephrotic syndrome, the patient with 522-kb deletion had collapsing focal segmental glomerular sclerosis (FSGS) phenotype, and the patient with 9-kb deletion displayed a milder minimal-change phenotype. These genetic data are supportive of a hypothesis for the involvement of the exocyst in human glomerular disease.

Injury to podocytes significantly down-regulated members of exocyst complex and its regulator Cdc42

To further determine whether the exocyst complex participates in podocyte injury, we performed mRNA profiling (RNA-Seq) of cultured podocytes treated with the glomerular injury-inducing agent puromycin aminonucleoside (PAN). The analysis showed significant down-regulation of multiple proteins (EXOC2–5 and -7) in response to injury (Fig. 1*D*). Interestingly, CDC42, a known regulator for the exocyst complex (12, 23, 24), was also down-regulated, further implicating involvement of the exocyst complex in podocyte injury.

Podocyte-specific KO of the central exocyst component, Exoc5, disrupted podocyte function and induced proteinuria

To investigate the role of exocyst in podocytes, the exocyst complex was disrupted by genetically deleting Exoc5 specifi-

[3] The abbreviations used are: SV, structural variation; NEPTUNE, Nephrotic Syndrome Study Network; Chr., chromosome; MAPK, mitogen-activated protein kinase; ERK, extracellular signal-regulated kinase; SNP, single-nucleotide polymorphism; FSGS, focal segmental glomerular sclerosis; SEM, scanning electron microscopy; TEM, transmission electron microscopy; TUNEL, terminal deoxynucleotidyltransferase–mediated dUTP nick end-labeling; TdT, terminal deoxynucleotidyltransferase; WGS, whole-genome sequencing; RPKM, reads per kilobase of exon model; FP, forward primer; RP, reverse primer; HBSS, Hanks' buffered salt solution; MUSC, Medical University of South Carolina; TGF-β, transforming growth factor-β; Seq, sequencing; GO, Gene ontology; Ab, antibody; GAPDH, glyceraldehyde-3-phosphate dehydrogenase; PAN, puromycin aminonucleoside; NTS, nephrotoxic serum; α-SMA, α-smooth muscle actin.

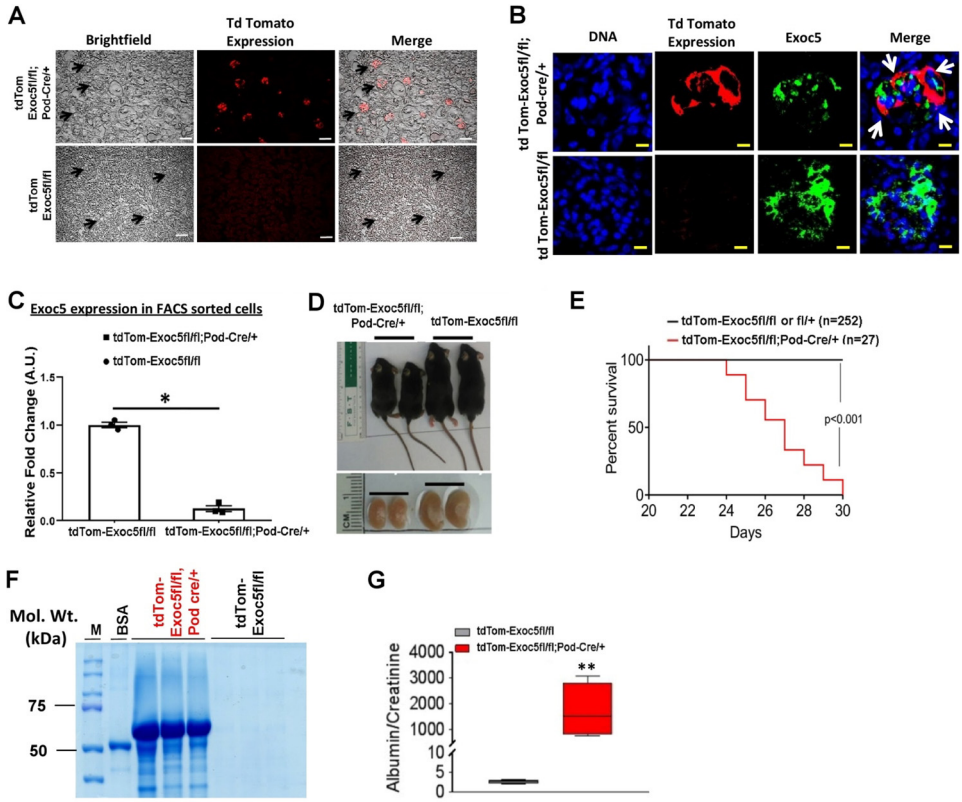

Figure 2. Podocyte-specific knockout of Exoc5. *A,* podocyte-specific Exoc5 KO mice on tdTomato background (tdTom–Exoc5fl/fl;Pod–Cre/+) showed tdTomato expression (*red color* without staining) in the glomerular podocytes (*black arrows*). There was no red Tomato expression in tdTom–Exoc5fl/fl glomeruli, where Cre had not been expressed. *Bar,* 100 μm. *B,* kidney sections from podocyte-specific Exoc5 KO mice, on a tdTomato background, stained with Exoc5 antibody (*green*) showed tdTomato expression (*red*) in podocytes (*arrows*), where Exoc5 was inactivated by Cre. Expression of Exoc5 (*green*) in glomerular cells other than podocytes was readily visible. *Bar,* 50 μm. *C,* RT-PCR confirming the loss of Exoc5 expression in podocytes isolated by FACS sorting from the glomeruli of podocyte-specific Exoc5 KO mice. (*, $p < 0.01$, paired *t* test.) *D,* podocyte-specific KO of Exoc5 (tdTom–Exoc5fl/fl;Pod- Cre/+) mice leads to stunted growth compared with littermate control (tdTom–Exoc5fl/fl) mice. Survival curve showed that all podocyte-specific Exoc5 knockout mice die within 30 days after birth (*E*), SDS-PAGE (*F*), and albumin/creatinine ratio (μg/μg) (*G*) showed massive proteinuria in podocyte-specific Exoc5 KO mice (tdTom–Exocfl/fl;Pod Cre/+) compared with control (tdTom–Exoc5fl/fl) mice.

cally in podocytes. Thus, the *Exoc5fl/fl* mouse line that we previously generated (25) was crossed with the Podocin–Cre driver mouse line (26). Ai14 Cre reporter mice that harbor a loxP-flanked STOP cassette preventing transcription of a CAG promoter-driven red fluorescent protein variant (tdTomato), congenic on the C57BL/6J genetic background, were mated with *Exoc5fl/fl* mice to induce tdTomato expression in a cell where Exoc5 has been inactivated by Cre. The target tdTom–Exoc5fl/fl;Pod–Cre/+ mice selectively labeled podocytes in which Exoc5 was deleted with red fluorescence (Fig. 2*A*). The kidney sections from these mice were stained with Exoc5 antibody, and as shown in Fig. 2*B*, the staining of Exoc5 did not overlap with the red fluorescence indicating Exoc5 deletion in podocytes. Additionally, the red podocytes were isolated by FACS sorting and subjected to quantitative PCR analysis, which showed more than 90% loss of Exoc5 (Fig. 2*C*). Collectively, these results confirmed genetic deletion of Exoc5 specifically in podocytes.

Podocyte-specific Exoc5 KO mice die within 1 month of birth due to renal failure

tdTom–Exoc5fl/fl;Pod–Cre/+ mice were born in normal Mendelian ratios but were significantly smaller in size when compared with their WT littermates (Fig. 2*D*), and all of them died within 30 days of birth (Fig. 2*E*). The SDS-PAGE analysis of urine samples from these mice showed significant amounts of albumin in tdTom–Exoc5fl/fl;Pod–Cre/+ mice, but not in tdTom–Exoc5fl/+;Pod–Cre/+ (data not shown) and tdTom–Exoc5fl/fl mice (Fig. 2*F*). Quantitative analysis further revealed massive proteinuria (Fig. 2*G*), indicating severe disruption of the glomerular filtration barrier. The histological analysis of tdTom–Exoc5fl/fl;Pod–Cre/+ mice showed altered glomerular structures with significant amounts of proteinaceous casts, a hallmark of proteinuria, whereas tdTom–Exoc5fl/+;Pod–Cre/+ and tdTom–Exoc5fl/fl mice displayed normal histology (Fig. 3*A*). The kidney sections of Exoc5fl/fl;Pod–Cre/+ mice were further analyzed by hematoxylin and eosin (*H&E*, Fig. 3*A*, *left panel*), periodic acid-Schiff (*PAS*, Fig. 3*A*, *middle panel*), and Masson's trichrome stains (Fig. 3*A*, *right panel*), which showed deposition of proteinaceous casts in tubules (*white arrows*), altered glomerular morphology (*black arrow*), and increased fibrosis (Masson's trichrome, Fig. 3*A*, *right two panels*) indicating significant injury to the glomeruli.

Podocyte-specific Exoc5 KO showed foot process effacement and loss of slit diaphragm

Podocyte foot process effacement is the hallmark of many glomerular diseases that affect podocyte structure and function, including FSGS (27–29). To further evaluate the effect of

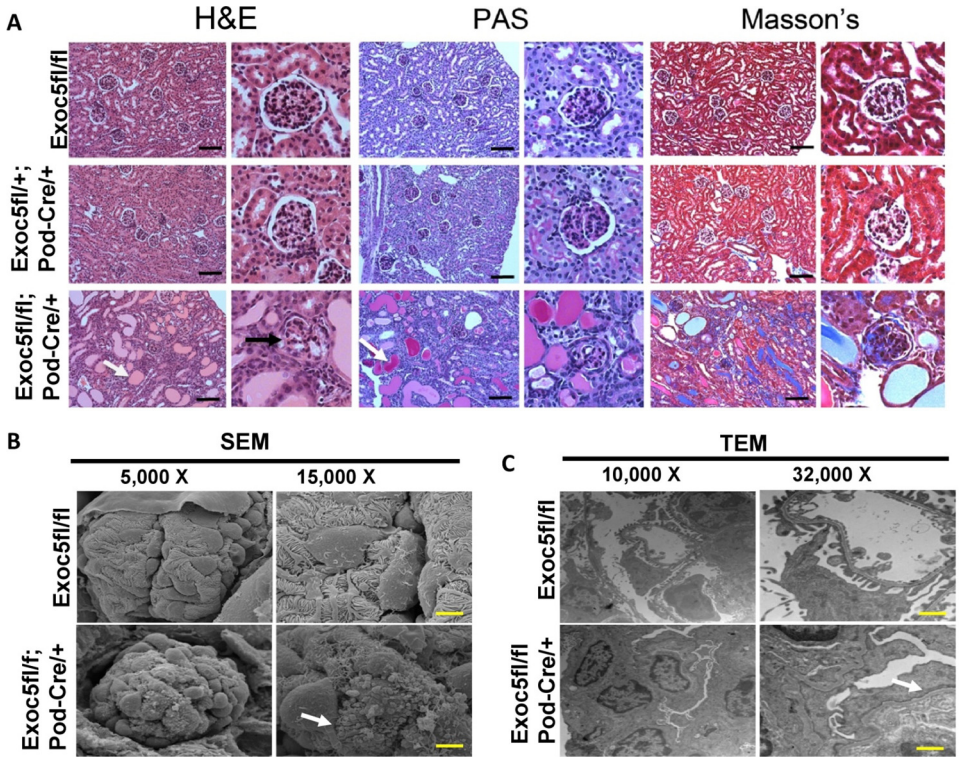

Figure 3. Histological and ultrastructural analyses. *A,* hematoxylin and eosin (*H&E*), periodic acid Schiff (*PAS*), and Masson's trichrome stains of kidney sections from podocyte-specific Exoc5 KO (Exoc5fl/fl;Pod–Cre/+) mice show proteinaceous casts in tubules (*white arrows*), altered glomerular morphology (*black arrow*), and increased fibrosis (*blue color* with Masson's trichrome) compared with the heterozygous podocyte-specific Exoc5 KO (Exoc5fl/+;Pod–Cre/+) and control (Exoc5fl/fl) mice. Higher magnification images to the *right of each panel* are 6×. The *blue color* depicts areas of fibrosis. *Bar,* 100 μm. *B* and *C,* ultrastructural (SEM) analysis of podocyte-specific Exoc5 KO glomeruli showed significant loss of foot processes (*white arrow*), and the TEM showed foot process fusion and loss of slit diaphragm (*black arrow*) when compared with the littermate controls. *Bars,* 1 μm.

Exoc5 deletion on podocyte structure, ultrastructural analyses of tdTom–Exoc5fl/fl;Pod–Cre/+ and control mice were performed using scanning (SEM) and transmission electron (TEM) microscopic procedures. Compared with the control littermates, the SEM images of Exoc5fl/fl;Pod–Cre/+ mice showed significant alterations to glomerular morphology, with loss of secondary and tertiary foot processes (Fig. 3*B*). In addition, the TEM analysis showed foot process fusion and effacement with loss of the slit diaphragm (Fig. 3*C*). These profound changes to podocyte structure suggest that loss of Exoc5 induces structural and functional damage to podocytes, and it may affect the development and/or maintenance of these cells.

Ciliogenesis does not contribute to the proteinuric phenotype in Exoc5 KO mice

Because multiple studies have shown the requirement of the exocyst complex for ciliogenesis in kidney tubule cells (10–13), we investigated whether ciliogenesis-based mechanisms contributed to this phenotype. Thus, we generated mice with podocyte-specific KO of a ciliary protein, intraflagellar transport protein 88 (Ift88) (Fig. 4*A*, *both panels*). Ift88 is required for ciliogenesis, and loss of this protein leads to the absence of cilia (30–32). Interestingly, the Ift88fl/fl:Pod-Cre/+ mice developed normally and did not show any signs of proteinuria or any renal abnormality even after 6 months of monitoring (Fig. 4*B*). These results indicate that exocyst mechanisms other than ciliogenesis contribute to the pathogenic phenotype observed in podocyte-specific Exoc5 KO mice. Additionally, the deletion of Ift88 in podocytes had no effect on sensitivity of mice toward glomerular injury induced by NTS and/or adriamycin (Fig. 4, *C* and *D*), further supporting the idea that ciliogenesis does not contribute to podocyte structure and/or function.

Exoc5 knockdown in cultured podocytes down-regulated intracellular movement and localization events

To further investigate the mechanism through which loss of Exoc5 results in podocyte damage, we generated Exoc5 knockdown cultured human podocytes using Exoc5-specific shRNA (Fig. 5*A*). The mRNA isolated from scramble control and Exoc5 knockdown podocytes were subjected to profiling analysis. RNA-Seq data were submitted to the Gene Expression Omnibus (GEO) database (accession number GSE127736). The *volcano plot* shows 3,921 differentially expressed genes in Exoc5 knockdown human podocytes, of which 1,661 were up-regulated and 2,260 were down-regulated (Fig. 5*B*). The heat map of hierarchical clustering from RNA-Seq data showed differentially expressed genes in control and Exoc5 knockdown podocytes cells (Fig. 5*C*). Gene ontology enrichment analysis was performed, which identified several major biological processes ($p < 0.05$), including cellular movement, apoptosis, locomotion, vesicle transport, and protein localization (Fig. 5*D* and Table 1). These data highlight the role of Exoc5 in cellular trafficking events in podocytes.

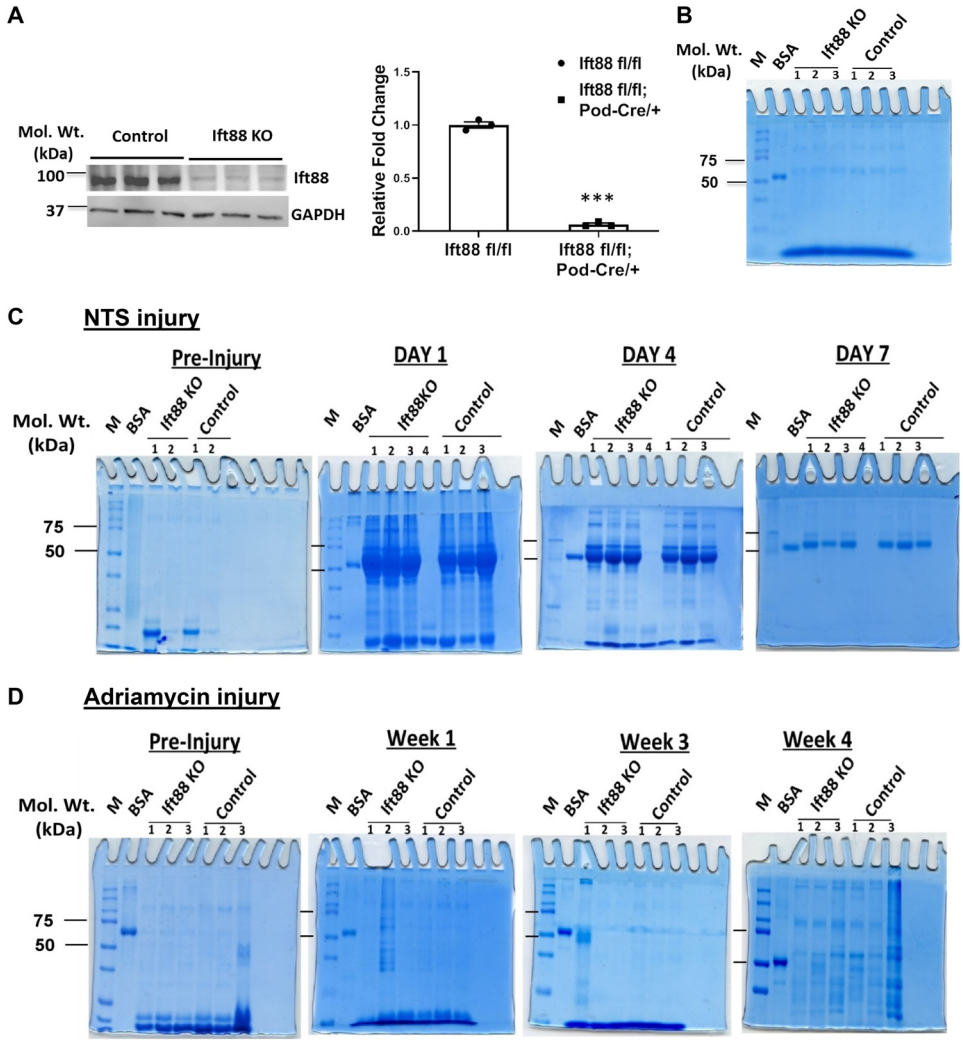

Figure 4. Podocyte-specific Ift88 knockout mice are not proteinuric and are not more susceptible to glomerular injury. *A,* podocyte-specific Ift88 knockout mice were generated (Ift88fl/fl;Pod–Cre/+). Immunoblot and RT-PCR analysis of glomeruli isolated from Ift88 KO and control mice. ***, $p < 0.001$. *B,* SDS-PAGE of the urine from Ift88 podocyte-specific KO mice showed no evidence of proteinuria. *C* and *D,* podocyte-specific Ift88 knockout and control mice (Ift88fl/fl;Pod–Cre/+) were subjected to acute (*NTS*) (*C*) and chronic (adriamycin) (*D*) glomerular injury, and the extent of albuminuria was assessed. No changes in albuminuria, compared with controls, were noted in either of these models.

Loss of Exoc5 induced mislocalization of slit diaphragm proteins Nephrin and Neph1

Because the mRNA-Seq analysis suggested involvement of Exoc5 in cellular transportation and localization events and the podocyte-specific Exoc5 knockout resulted in loss of the slit diaphragm leading to podocyte dysfunction, we hypothesized that Exoc5 is involved in trafficking of the slit diaphragm proteins Nephrin and Neph1. Because the slit diaphragm is a modified cell junction, which is constructed through homo- and heterophilic interactions between Nephrin and Neph1 (33, 34), we further hypothesized that the loss of the slit diaphragm in Exoc5fl/fl;Pod–Cre/+ mice was due to mislocalization of Nephrin and Neph1. Indeed, immunofluorescence analysis of kidney sections from these mice showed significant changes to the distribution of Neph1 and Nephrin. Both proteins failed to colocalize with the podocyte marker synaptopodin in Exoc5fl/fl;Pod–Cre/+ mice (Fig. 6*A*). To further validate these observations, Exoc5 knockdown podocyte cells were generated, which in addition to the loss of Exoc5 showed down-regulation of the other exocyst components, except for Exoc6 (Fig. 6*B*). When analyzed, these cells showed an increase in Neph1, SMAD3, and ERK phosphorylation, which indicates progression of injury (Fig. 6, *C* and *D*) and is consistent with previous reports in which injury induced Neph1 phosphorylation (35). Induction of glomerular injury is known to activate the MAPK (ERK) pathway (36, 37), and we previously showed that knockout of Exoc5 in kidney tubules increased MAPK expression (10, 13, 25). Here, we note a similar increase for ERK phosphorylation in Exoc5 KD podocytes (Fig. 6*C*).

The induction of fibrosis in the kidney sections from Exoc5 knockout mice (Fig. 3*A*) prompted us to investigate whether the loss of Exoc5 affects TGF-β signaling. Hence, immunoblot analysis of cell lysate from the Exoc5 KD cultured podocytes was performed, which showed increased expression of α-SMA and phosphorylated SMAD3 (Fig. 6*C*). A similar increase in the expression of phosphorylated SMAD3 was also noted in the Exoc5 knockout zebrafish line (Fig. S1). Collectively, these results highlight a mechanism that involves activation of

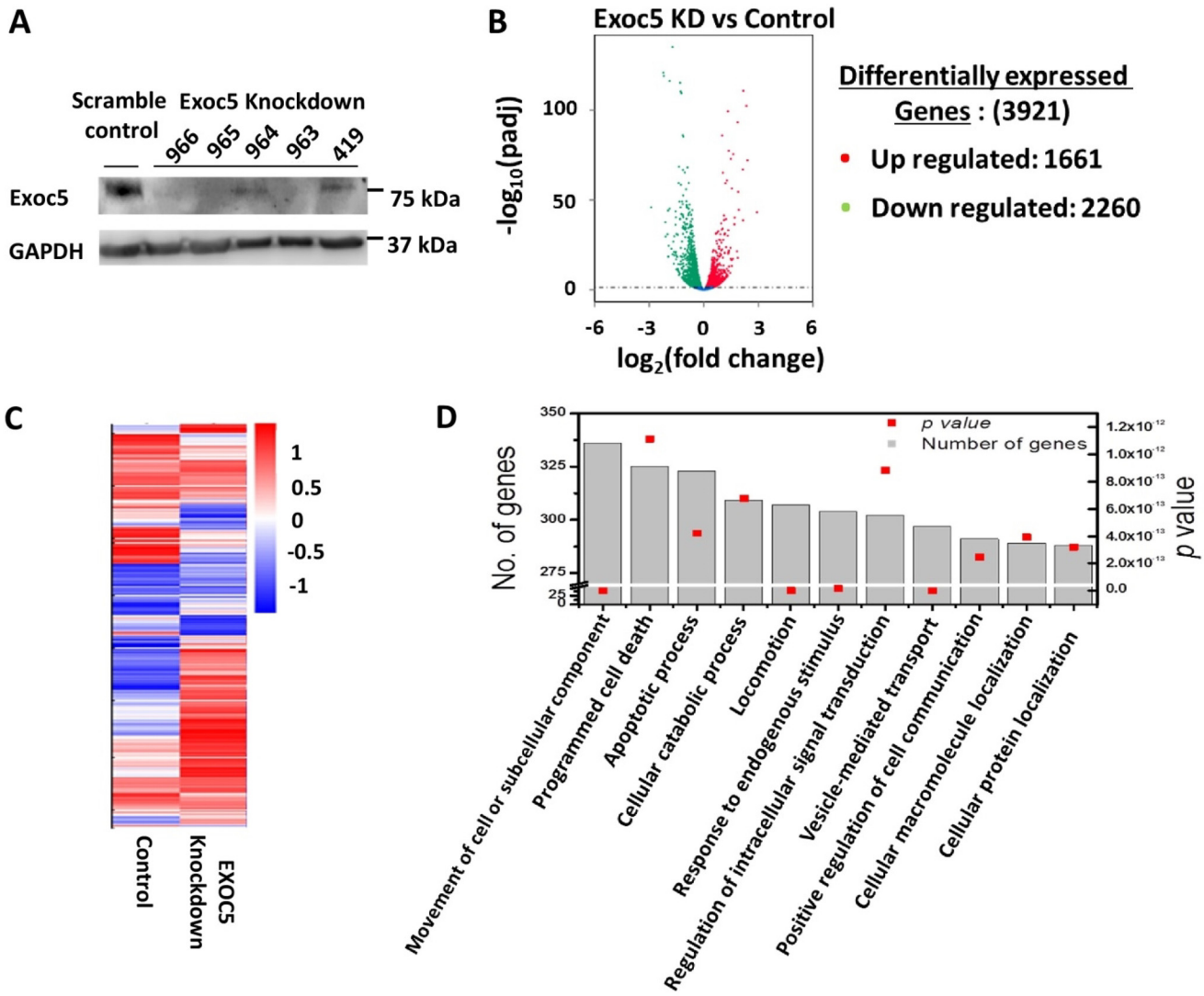

Figure 5. Exoc5 KD in cultured podocytes and RNA-Seq. *A,* immunoblot analysis of Exoc5 protein levels in various Exoc5 KD clones. *B, volcano plot* of differentially expressed genes from control and Exoc5 knockdown cells. *C,* heat map of hierarchical clustering from RNA-Seq data showed differentially regulated genes in Exoc5 knockdown and control podocytes. The adjusted *p* values (≤0.05) using Benjamin and Hochberg's approach that were reported by DESeq2 and assigned to the differentially regulated genes are shown. $n = 3$ experimental replicates. *D,* GO enrichment analysis showed multiple cellular trafficking events (presented as histograms) that were enriched in response to Exoc5 knockdown.

canonical and noncanonical TGF-β signaling pathways that may contribute to the disease phenotype.

To further confirm that the loss of Exoc5 affects the expression of Exoc4 (also known as Sec8) in these podocytes, immunoblotting was performed, which showed significant down-regulation of Exoc4 in these cells (Fig. 6, *C* and *D*). Thus, these results are in agreement with our previously published results showing that loss of Exoc5 destabilizes the exocyst complex, most likely leading to its degradation (13). These results further validate Exoc5 as the central exocyst component.

Additional analysis of Exoc5 KD podocytes showed significant reduction in the localization of Neph1 at the podocyte cell membrane providing further support for the role of Exoc5 in trafficking (Fig. 7, *A* and *B*). Because Nephrin protein remains undetectable in cultured podocytes, similar analyses could not be performed for endogenous Nephrin. To further confirm these observations, we constructed chimeric Nephrin and Neph1 constructs, where a FLAG-tag was inserted in the extracellular domain of these proteins, immediately following the signal peptide sequence, but before the functional IgG domains (Fig. 7*C*). These constructs were transfected into Exoc5 KD podocytes, and their surface/membrane localization in live cells was assessed using FLAG antibody (Fig. 7, *D* and *G*). Similar to our *in vivo* results, a significant reduction in membrane localization of Nephrin and Neph1 was noted in Exoc5 KD cultured podocytes (Fig. 7, *E, F, H,* and *I*). These data support the hypothesis that Exoc5 regulates trafficking of slit diaphragm proteins Neph1 and Nephrin.

Importantly, the loss of Neph1 and Nephrin membrane localization in human Exoc5 KD podocytes was rescued by transducing cells with packaged viruses expressing WT mouse Exoc5 (Fig. 8), which was not susceptible to the shRNA given a difference in primary base-pair structure (Fig. S2).

To further demonstrate the effect of Exoc5 on the trafficking of slit diaphragm proteins, we examined the movement of Neph1 vesicles in cultured podocytes. To do this, we generated

Table 1
Table shows the top 20 biological pathways affected and the number of genes down-regulated following knockdown of EXOC5 in cultured podocytes (as determined by GO TERM analysis of the RNA-Seq data)

Biological process	No. of genes down-regulated	*p* value
Movement of cell or subcellular component	336	1.68E-17
Programmed cell death	325	1.11E-12
Apoptotic process	323	4.21E-13
Cellular catabolic process	309	6.78E-13
Locomotion	307	1.93E-15
Response to endogenous stimulus	304	1.51E-14
Regulation of intracellular signal transduction	302	8.83E-13
Vesicle-mediated transport	297	1.83E-21
Positive regulation of cell communication	291	2.47E-13
Cellular macromolecule localization	289	3.94E-13
Cellular protein localization	288	3.20E-13
Positive regulation of signaling	287	4.04E-13
Regulation of cell death	285	4.80E-13
Biological adhesion	284	1.36E-16
Positive regulation of protein metabolic process	282	1.28E-13
Cell adhesion	280	5.43E-16
Positive regulation of multicellular organismal process	279	5.99E-13
Cell motility	271	1.43E-17
Localization of cell	271	1.43E-17
Regulation of programmed cell death	268	8.41E-13

cultured podocytes stably expressing mCherry–Neph1 (Fig. S3). Exoc5 was knocked down in these podocytes, and the movement (micrometers) and speed (micrometers/s) of mCherry–Neph1 vesicles were evaluated. The results showed that loss of Exoc5 significantly decreased the movement and speed (~30 and ~20% respectively) of mCherry–Neph1 vesicles as shown by time-lapse live-cell imaging analysis (Fig. 9, *A* and *B*).

Podocyte-specific Exoc5 knockout induced apoptosis in podocytes

Because podocyte loss leads to proteinuria (38) and our mRNA profiling analysis indicated apoptosis as a major cellular event in Exoc5 KD podocytes, we investigated whether Exoc5 deletion induced apoptosis in podocytes. Indeed, TUNEL staining of kidney sections showed increased apoptotic nuclei in Exoc5fl/fl;Pod–Cre/+ mice, when compared with the control mice (Fig. 10, *A* and *B*). Interestingly, apoptotic nuclei were also observed in cells surrounding the glomeruli. This is not totally surprising given the fact that there is significant cross-talk between podocytes and other glomerular cell types, including endothelial cells and the glomerular basement membrane (39).

Discussion

We report several novel findings in this study. Importantly, this is the first study to examine the role of the exocyst complex in podocyte development and disease. The hypothesis for involvement of the exocyst was prompted by the discovery of two rare heterozygous deletions impacting EXOC4 in patients with nephrotic syndrome that were not seen in a reference population of 2,504 individuals. Independent support for the genetic dependence on the exocyst for podocyte development and/or health was demonstrated in mice using podocyte-specific KO of Exoc5. Loss of Exoc5 in podocytes resulted in significant glomerular damage leading to death in all mice within 30 days of birth. Whether exocyst inhibition prevents normal development of the podocytes, inhibits podocyte homeostasis, or both, is something that needs to be studied further using timed matings.

Signaling of Nephrin and Neph1 is a critical event that governs subsequent trafficking of these proteins in response to injury. Our results indicate that Exoc5 and the exocyst may participate in regulating the signaling of slit diaphragm proteins, particularly Nephrin and Neph1. To determine whether ciliogenesis contributed to the pathogenic phenotype in Exoc5 KO mice, we generated mice with podocyte-specific KO of the ciliary protein Ift88. Many reports have shown that Ift88 is required for ciliogenesis, and loss of this protein leads to the absence or severe stunting of primary cilia (30, 40). Interestingly, these mice remained healthy and showed no signs of proteinuria or increased susceptibility to glomerular injury, indicating that exocyst-mediated mechanisms other than ciliogenesis contributed to the pathogenic phenotype that we observed in Exoc5 KO mice.

Previous studies using various injury models have shown that glomerular injury induces redistribution of slit diaphragm proteins Nephrin and Neph1, which is associated with podocyte dysfunction and proteinuria (5, 41, 42). Our podocyte-specific Exoc5 KO mice showed similar results suggesting that loss of Exoc5 replicated events that cause podocyte injury. Because Nephrin and Neph1 have been shown to be critical for podocyte survival, and loss of Exoc5 significantly affected Nephrin and Neph1 expression and localization, we hypothesized that the exocyst plays a major role in regulating their trafficking and signaling, thus affecting podocyte development and/or maintenance. The role of Exoc5 in the trafficking of Nephrin and Neph1 was further substantiated using cultured human Exoc5 knockdown podocytes, where loss of Exoc5 significantly attenuated the membrane localization of chimeric Nephrin and Neph1 proteins. Moreover, the profiling analyses of Exoc5 knockdown podocytes further confirmed trafficking as the major cellular event affected due to loss of Exoc5. Thus, it is likely that trafficking associated events are the major contributor to the proteinuric phenotype observed in Exoc5 knockout mice.

Glomerular injury-induced Neph1 phosphorylation and induction of the MAPK pathway have been reported previously (43), and similar observations were noted in our Exoc5 knockdown cells. Although little is known about the signaling events that are initiated in response to Nephrin and Neph1 activation, the phosphorylation and therefore the induction of both Neph1 and Nephrin, and the MAPK pathway in Exoc5 KO mice, provide evidence for the participation of the exocyst in generating the injury phenotype. Importantly, our results also showed that TGF-β signaling is induced in Exoc5 knockdown podocytes. Although TGF-β is known to participate in podocyte pathogenesis (44–46), the results from this study suggest that Exoc5 may negatively regulate TGF-β signaling. However, these conclusions need to be investigated further through a detailed analysis of TGF-β signaling in Exoc5-depleted and -overexpressing systems, which will be the subject of future investigations.

We previously demonstrated that Cdc42 regulates the exocyst complex (12, 23, 24), and it is interesting to note that our podocyte-specific Exoc5 KO mice phenocopied podocyte-specific Cdc42 KO mice (47). Based on these results, and the over-

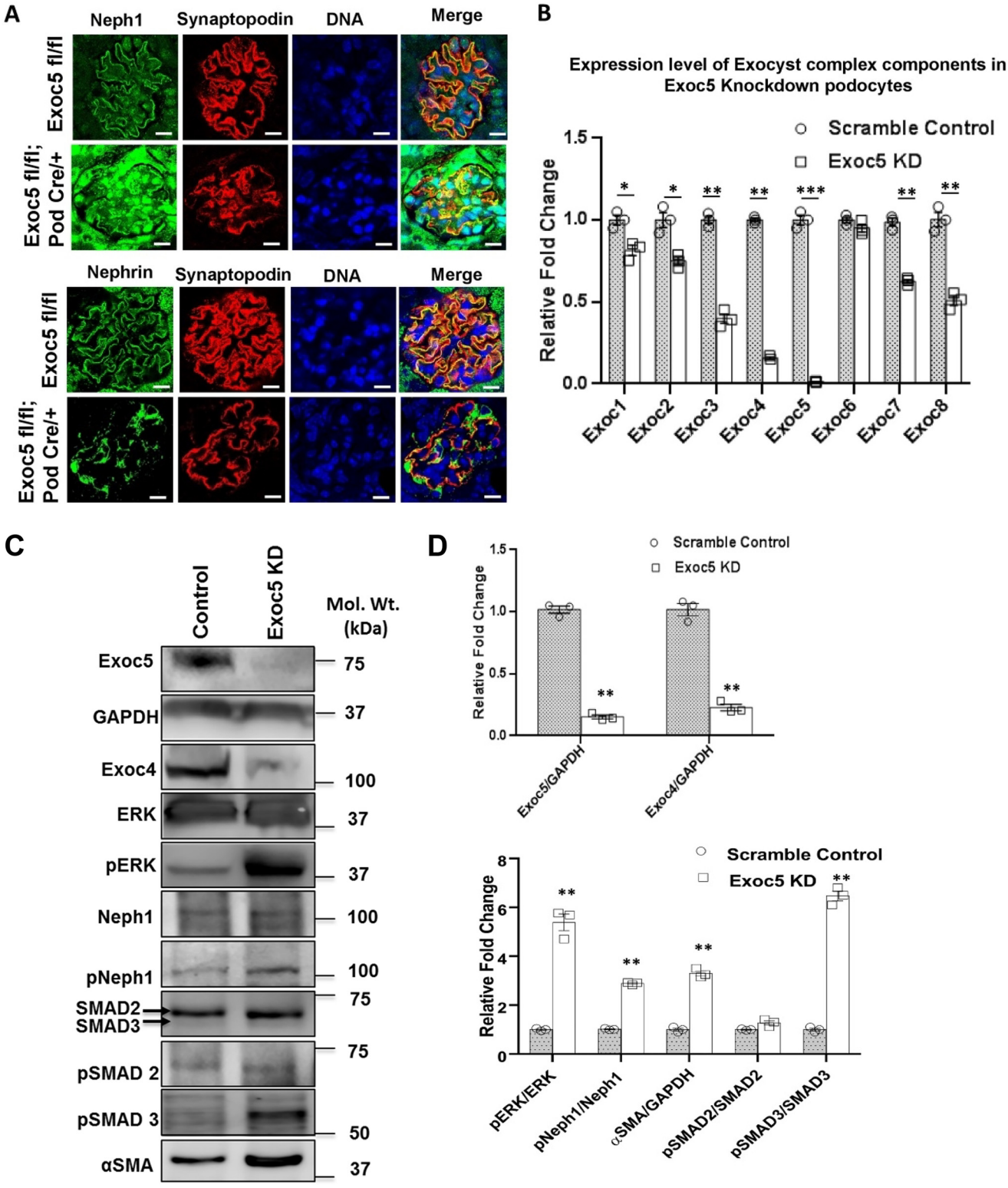

Figure 6. Podocyte-specific Exoc5 deletion alters Nephrin and Neph1 expression/localization. *A,* there was significant mislocalization of Nephrin and Neph1 (*green*) in podocyte-specific Exoc5 KO (*Exoc5fl/fl*;Pod-Cre/+), compared with littermate control (tdTom–*Exoc5fl/fl*), glomeruli. Nephrin and Neph1 normally colocalize (merged images) with synaptopodin (*red*). *Blue color* represents 4′,6-diamidino-2-phenylindole–stained nuclei. *Bar,* 10 μm. *B,* expression analysis for various exocyst components in human Exoc5 KD podocytes using RT-PCR. *C,* Western blot analysis of Exoc5 KD podocytes showed increased ERK, SMAD3, and Neph1 phosphorylation along with concomitant loss of Exoc4 expression. *D,* relative protein quantification from *C*. **, $p < 0.01$, paired Student's *t* test.

all results presented in this study, we hypothesize that fundamental mechanisms that regulate trafficking of slit diaphragm proteins also regulate podocyte structure and function. These data, for the first time, identify the exocyst as a novel component of podocytes that actively participates in their development and/or homeostasis.

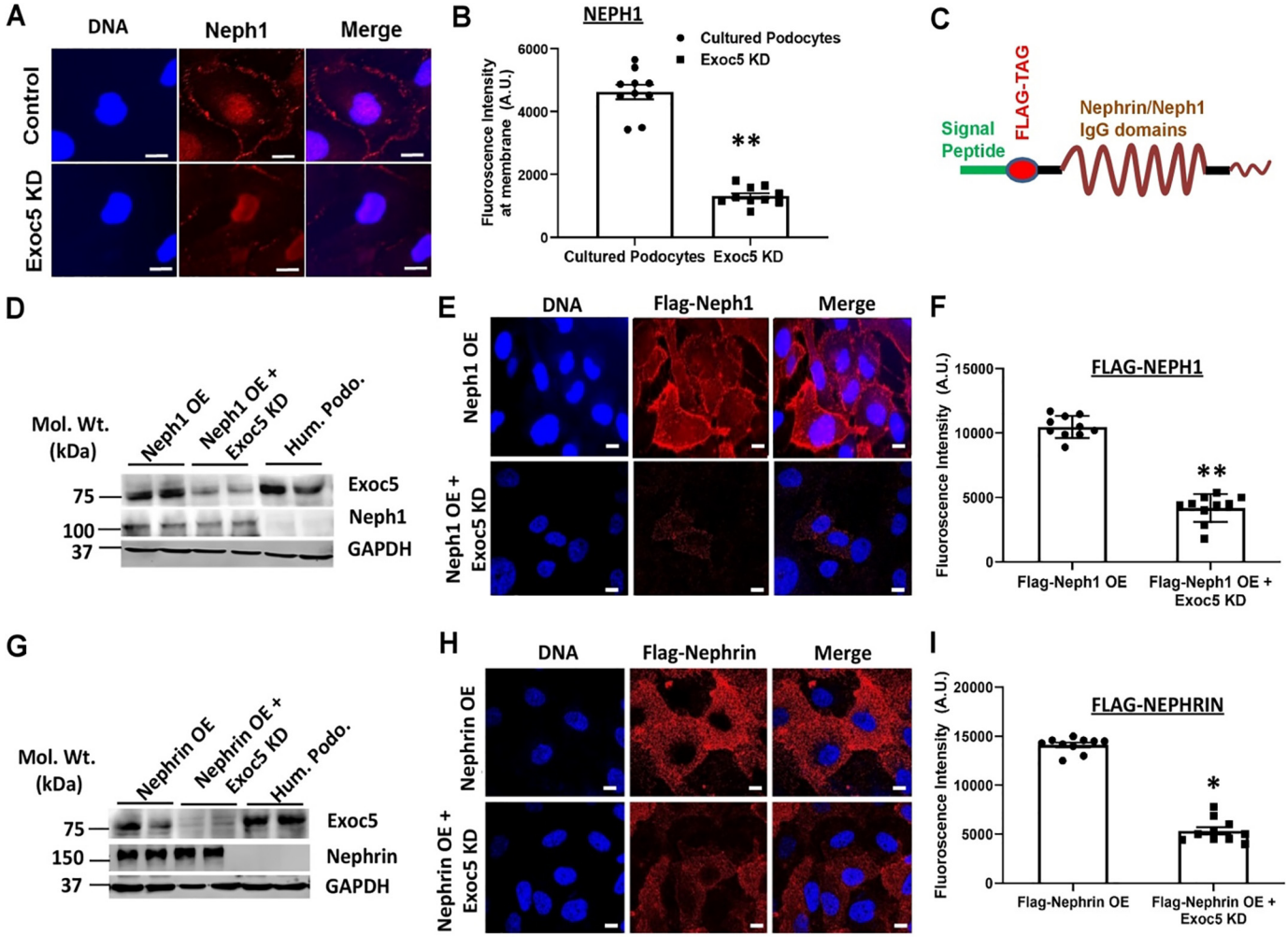

Figure 7. Slit diaphragm proteins Nephrin and Neph1 are mislocalized in Exoc5 KD podocytes. *A* and *B*, membrane localization of endogenous Neph1 at the cell–cell junctions was reduced in Exoc5 KD podocytes. *Bar*, 5 μm. 4′,6-Diamidino-2-phenylindole -stained nuclei (DNA) are shown in *blue* ($n = 10$). *C*, schematic of the chimeric Neph1 and Nephrin constructs, where FLAG-tag was inserted following the signal peptide sequence. *D–I*, chimeric Nephrin and Neph1 were expressed in cultured podocytes (*D* and *G*), and stable cell lines were created. Nephrin and Neph1 in these cells were extracellularly labeled with FLAG antibody and live-cell staining was performed. The surface localization of Neph1 and Nephrin was analyzed by immunofluorescence using confocal microscopy (*E* and *H*), and the images were quantified using ImageJ, which showed significant loss of surface Neph1 and Nephrin in Exoc5 knockdown podocytes ($n = 10$) (*F* and *I*). *Bar*, 25 μm. In each experiment, 2 million cells were plated on each coverslip, and 10 or more cells were analyzed for quantification and statistical analysis. **, $p < 0.001$; *, $p < 0.01$, paired Student's *t* test.

Materials and methods

Structural variation analysis

We used low-depth whole-genome sequencing (WGS) and Illumina Infinium Exome genotypes that were collected from the NEPTUNE patients. SV calls from WGS were made by the GenomeSTRiP pipeline, and we looked for those that affected an exon(s) and were not present in participants from the 1,000 Genome Project Phase 3, which we used as a reference (48). For independent confirmation of this finding, we examined intensities of the *EXOC4* SV region using the Exome Chip genotypes.

Generation of podocyte-specific Exoc5 knockout mice

To investigate the role of the exocyst in podocytes, we generated podocyte-specific Exoc5 KO mice by crossing Exoc5fl/fl with Podocin–Cre (Pod–Cre) mice on a C57BL6/J background. Target mice, designated Exoc5fl/fl;Pod–Cre/+, were confirmed by PCR-based genotyping. Genotyping primers used were GCCTGTAACTCACAGAGATC (forward) and GCTGGCATTCTAAGTCATGG (reverse) for Exoc5 flox and AGGTTCGTGCACTCATGGA (forward) and TCGACCAGTTTAGTTACCC (reverse) for Cre recombinase. To further demonstrate the fidelity of Cre recombinase, Exoc5fl/fl mice were mated with Ai14 Cre reporter mice that harbor a loxP-flanked STOP cassette preventing transcription of a CAG promoter-driven red fluorescent protein variant (tdTomato), congenic on a C57BL/6J genetic background. This allowed expression of tdTomato in podocytes where Exoc5 was inactivated by Cre. The tdTomato expression was seen in tdTom–Exoc5fl/fl;Pod–Cre/+ and tdTom–Exoc5fl/+;Pod–Cre/+, but not in tdTomato Exoc5fl/fl, mice (Fig. 2). Urinalysis was performed by SDS-PAGE, and histological and morphological analysis of kidney sections using immunofluorescence and histological procedures. A similar strategy was followed to generate podocyte-specific Ift88 KO mice by crossing Ift88fl/fl with Pod–Cre mice on a C57BL6/J background to determine whether ciliogenesis is required for podocyte growth and development.

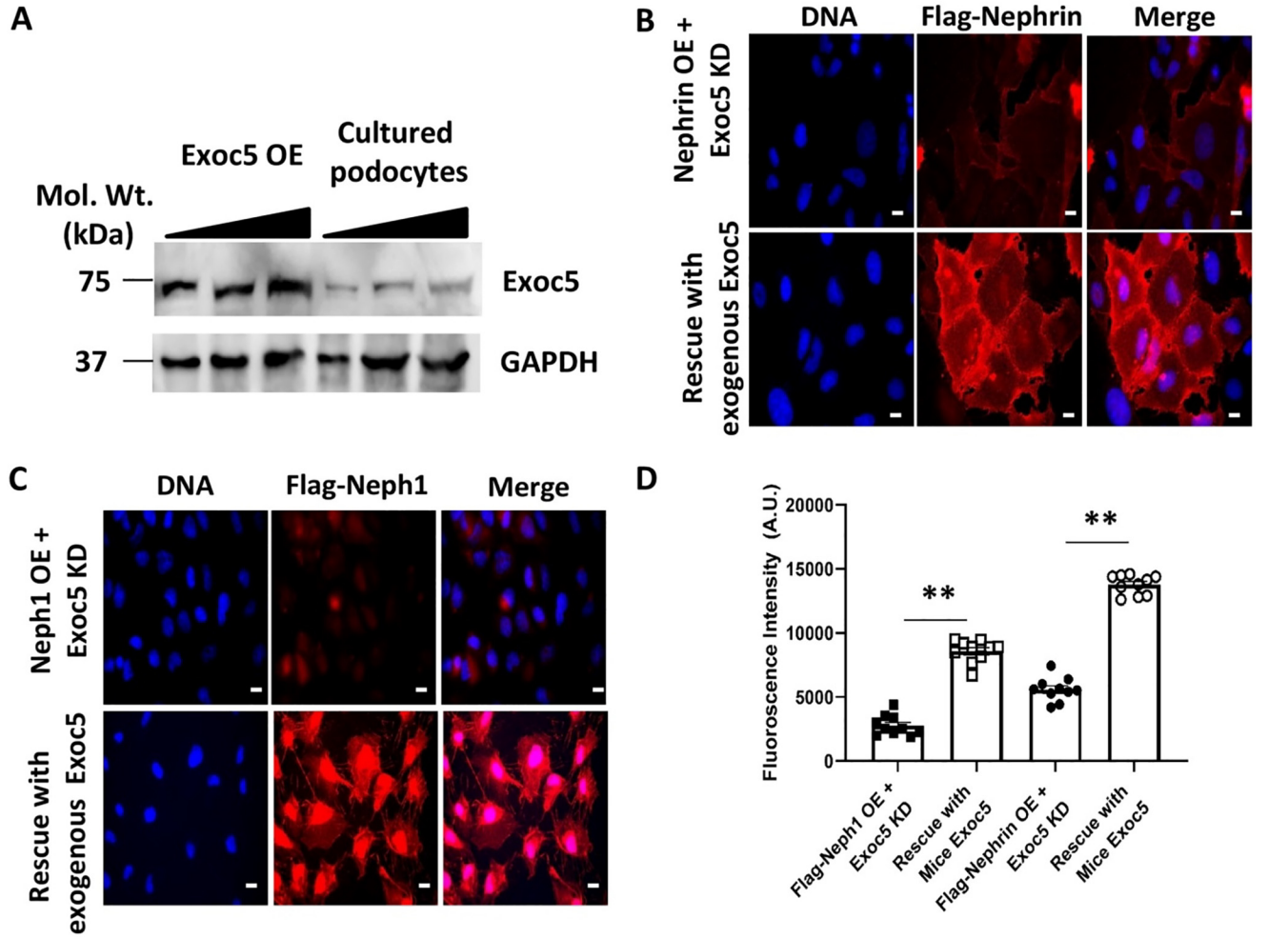

Figure 8. Overexpression of Exoc5 rescued loss of Nephrin and Neph1 localization in Exoc5 KD podocytes. A lentiviral expression construct of mouse Exoc5 was used to rescue Exoc5 KD in cultured human podocytes. *A,* Western blot analysis of Exoc5 overexpression in Exoc5 KD podocytes. *B* and *C,* cultured stable podocytes overexpressing FLAG-tagged Nephrin (*B*) and Neph1 (*C*) in Exoc5 KD podocytes were treated with lentiviral particles expressing mouse Exoc5, and surface staining was performed using anti-FLAG antibody. The localization of Nephrin (*B*) and Neph1 (*C*) to the podocyte cell membrane was restored in podocytes following exogenous expression of mouse Exoc5. *D,* quantification of fluorescence in *B* and *C* is shown ($n = 10$). *Bar,* 25 μm. (**, $p < 0.001$, paired Student's *t* test.) In each experiment, 2 million cells were plated on each coverslip, and 10 or more cells were analyzed for quantification and statistical analysis.

Histological and immunological characterization of Exoc5fl/fl; Pod–Cre/+ mice

Murine kidneys were perfused with Hanks' buffered salt solution (HBSS) for 5 min followed by 4% paraformaldehyde in HBSS for 15 min at 80–100 mm Hg retrograde to the intrarenal aorta of anesthetized mice using a 24-gauge angiocatheter (BD Biosciences). Mice were anesthetized with Avertin (2,2,2-tribromoethanol) before the procedure. Perfused kidneys were decapsulated, washed with 1× PBS, transected, fixed for 4–12 h in 4% paraformaldehyde, and rinsed, and sequential alcohol treatments were performed. The samples were submitted to the Abramson Histology Core at MUSC and the University of South Carolina's Histology Core facility. Paraffin-embedded sections were obtained and deparaffinized with xylene-ethanol (EtOH). Paraffin-embedded sections were stained with Masson's trichome for histological analysis. Staining of various proteins, including Neph1, Nephrin, and synaptopodin, was performed using specific antibodies as described previously (49, 50). Briefly, antigen retrieval was performed using 10 mM Tris, 1 mM EDTA (pH 9.0) at 65 °C for >18 h. Kidney sections were encircled by use of a Pap pen, blocked in TBS, 0.025% Triton X-100 (TBST) plus 3% bovine serum albumin (BSA), incubated with primary antibody (Ab), washed five times, re-blocked with TBST plus 10% goat serum (Invitrogen) plus 1% BSA, incubated with Alexa Fluor secondary Ab (Invitrogen) at 1:1,000), washed five times, and mounted with Prolong Gold antifade reagent (Invitrogen). IgG control primary antibody were used as negative control (Fig. S4). A Zeiss inverted microscope (Zeiss Axio Observer D1m) fitted with ×63 and ×25 oil immersion objectives was used for fluorescence microscopy, whereas confocal microscopy was performed at MUSC on a Leica microscope. All parameters were maintained at a constant level throughout acquisition of the images, including the exposure time, and the images were collected in 16-bits format. ImageJ software was used for quantitative analysis. Multiple images from three or more mice were used for the quantitative analysis. Representative images from three or more independent experiments were used in each figure. For SEM and TEM analyses, the kidney samples were kept in a mixture of 2% glutaraldehyde and 2% paraformaldehyde solution overnight for fixation. Samples

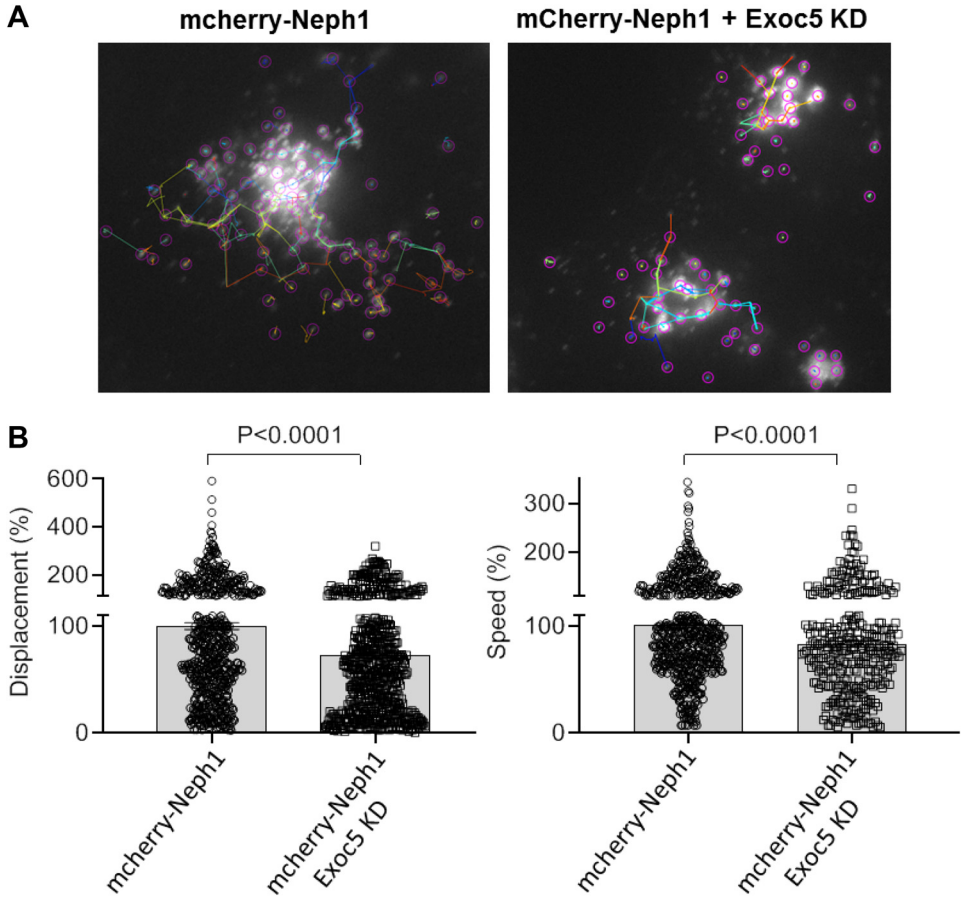

Figure 9. Exoc5 KD podocytes display reduced movement of cherry-Neph1 vesicles. *A,* podocytes expressing mCherry–Neph1 on a WT or Exoc5 KD background were plated on a glass-bottom cell culture plate, and the movement of Neph1-containing vesicles was analyzed using time-lapse live imaging. The vesicular movement was plotted as displacement (micrometers, *y* axis) *versus* time (seconds, *x* axis). *B,* decreased displacement (micrometers) and speed (micrometers per second) of mCherry–Neph1 vesicles were noted in the Exoc5 KD podocytes ($p < 0.0001$). Data are presented as means ± S.E.

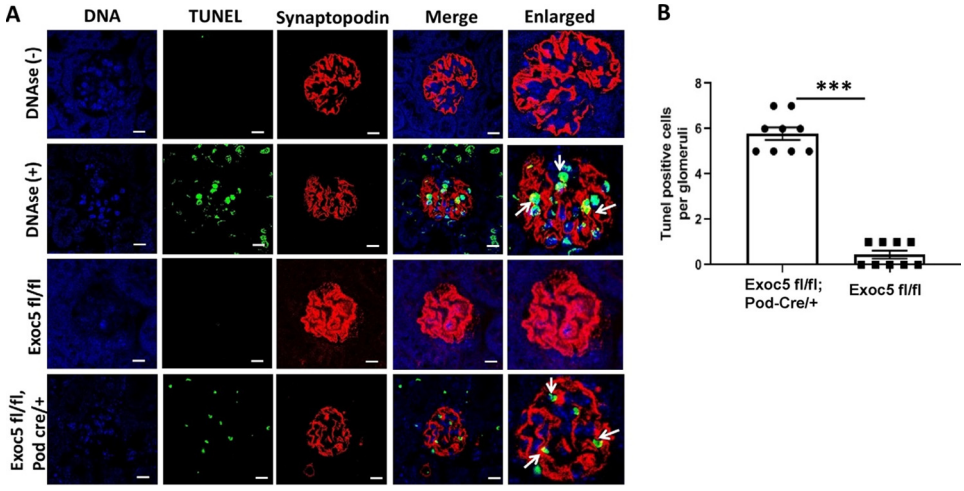

Figure 10. Exoc5 deletion induces apoptosis. *A* and *B,* significant amounts of TUNEL-positive nuclei were seen in the glomeruli of podocyte-specific Exoc5 knockout mice, but they were absent in the control mice. *Bar,* 20 μm ($n = 10$, ***, $p < 0.001$, paired Student's *t* test).

were processed, sectioned, and imaged at the Department of Pathology, MUSC. Five to 10 glomeruli per sample from at least three mice were evaluated, and slit diaphragm frequency and thickness of glomerular basement membranes were assessed quantitatively by counting the number of junctions/micron of basement membrane using ImageJ software.

Immunoblotting, antibodies, and reagents

Primary kidney cells and human podocytes were lysed in RIPA buffer, and protein estimation was performed using the BCA method. 20-μg protein samples from lysate were used for immunoblotting experiments. To ensure equivalent protein loading, the membranes were simultaneously incubated with

GAPDH mAb from Sigma (1:10 000) at 4 °C overnight. Membranes were washed three times with TBST, incubated with horseradish peroxidase–conjugated secondary antibodies (Pierce) at 1:10,000 dilutions for 1 h at room temperature, and washed extensively before detection. The membranes were subsequently developed using SuperSignal West Femto maximum sensitivity substrate (Pierce, catalog no. 34095), and images were collected using a LI-COR image analyzer, and densitometry analysis was performed at the LI-COR imaging station. Polyclonal purified antibodies to Neph1 and Nephrin have been previously described (5, 51). Other antibodies, such as GAPDH (Sigma, catalog no. G8795), α-SMA (Santa Cruz Biotechnology, catalog no. c-53142), phospho-ERK1/2 (Cell Signaling Technology, catalog no. 9101), and ERK1/2 (Cell Signaling Technology, catalog no. 4695S) were commercially obtained. The fluorophore secondary antibodies Alexa Fluor 488 goat anti-rabbit IgG (H+L), Alexa Fluor 568 goat anti-mouse IgG (H+L), and Alexa Fluor phalloidin were commercially obtained from Invitrogen.

Cell culture

The immortalized human podocyte cell line was obtained from Dr. Moin Saleem (52). The human podocyte cell line was cultured in RPMI 1640-based medium supplemented with 10% fetal bovine serum (Corning), insulin/transferrin/selenium supplement (Sigma), and 200 units/ml penicillin and streptomycin (Roche Applied Science), as described previously (53, 54).

shRNA-based Exoc5 knockdown in cultured podocytes

Exoc5 knockdown in cultured human podocytes was achieved using Exoc5-specific shRNA. To target Exoc5, we screened Mission Lentiviral Transduction particle shRNAs in pLKO.1-puro (Exoc5 MISSION Lentiviral Transduction shRNA particle, commercially purchased from Sigma, catalog no. SHCLNV-NM_006544 and TRC no. TRCN0000061963, TRCN0000061964, TRCN0000061965, TRCN00000286419, and TRCN0000061966). Transfection of the shRNA plasmids was performed with Lipofectamine 2000 (Invitrogen) according to the manufacturer's instructions. Transfected cells were grown in 2.5 μg/ml puromycin-containing medium for the selection of stable transfectants, and the Exoc5 knockdown was confirmed by Western blotting.

Generation of viral expression constructs for FLAG-Nephrin, FLAG-Neph1, mcherry Neph1, and mouse Exoc5

A standard PCR-cloning technique was used to generate the mammalian expression plasmid encoding FLAG-tagged full-length Nephrin in the pBABE-puro vector as described previously (55). The FLAG tag was inserted between the signal peptide and the start of the extracellular domains of Nephrin. The PCR-amplified FLAG-Nephrin was cloned at the EcoRI site in the retroviral vector pBABE-puro. The following two forward and one reverse primer sets were used for cloning: forward primer (FP) 1: 5′-CCCTGCTGCTCGCGGGAATGCTGACCACAGGCCTGGCCCAGTCGGACTACAAGGATGACGATGACAAACCAGTCCCCACCTCAGCACC-3′, FP 2: 5′-ATGGGAGCTAAGGAAGCCACAGTCAGAGGCCCCGGGGCAAGCCCAGTGCACAGAACTTGCCACCTGATTCCCCTGCTGCTCGCGGGAATGC-3′, and reverse primer (RP): 5′-AGGAATTCCATCACACCAGATGTCCCCTCAG-3′, respectively. The fidelity of the constructs was determined by restriction digestion and DNA sequencing. Neph1 was also cloned into the pBABE vector at the EcoRI and SalI site employing a similar strategy using following sets of primers: FP 5′-GAATTCATGACTCTGGAGAGCCCTAGCACA-3′ and RP as CGAGTCGACCTACACGTGAGTCTGCATGCG. Subsequently, the FLAG tag was inserted between the signal peptide and the extracellular domain of Neph1 using the following sets of primers: forward primer GACTACAAGGATGACGATGACAAAACTCAGACTCGCTTC and reverse primer TTTGTCATCGTCATCCTTGTAGTCCCCGGGCAAAGCCAA. Finally, retroviruses overexpressing FLAG-Neph1 and FLAG-Nephrin were generated by the transfection of the respective plasmids (cloned into the pBABE vector) into Phoenix cells according to the manufacturer's instructions. The cultured podocytes were transfected with these viruses, and the expression of FLAG-Nephrin and FLAG-Neph1 was evaluated by Western blotting. mCherry Neph1 was constructed in a pBABE Puro retroviral vector using standard PCR-cloning strategies, as described previously (55). Similarly, the lentiviral construct, where Exoc5 was cloned into the EcoRV site of the pLenti-GIII-UbC vector, was commercially obtained from Applied Biological Materials (ABM, Canada). Viruses expressing mouse Exoc5 were generated as per the manufacturer's instructions and used in the rescue experiment to express mouse Exoc5 in Exoc5 KD human cultured podocytes. The differences in the CDS sequences of mouse and human Exoc5 targeted by the shRNA lentiviral constructs were analyzed and are presented in Fig. S2.

Isolation of murine glomeruli

Mice were anesthetized using isoflurane and perfused with 8×10^7 Dynabeads diluted in 40 ml of PBS through the heart. Before the perfusion, the right atrium was cut to achieve the open circulation during perfusion. The kidneys were removed, minced into 1-mm^3 pieces, and digested in collagenase (1 mg/ml collagenase A, 100 units/ml DNase I in PBS) at 37 °C for 15 min with gentle agitation. The collagenase-digested tissue was gently pressed through a 70-μm cell strainer using a flattened pestle, and the cell strainer was then washed with 50 ml of PBS. The filtered cells were passed through a new 40-μm cell strainer without pressing, and the cell strainer was washed with 50 ml of PBS. The cell suspension was then centrifuged at 200 × *g* for 5 min. The supernatant was discarded, and the cell pellet was resuspended in 2 ml of PBS. Finally, glomeruli containing Dynabeads were gathered by a Magnetic Particle Concentrator and washed at least three times with PBS. During the procedure, kidney tissues were kept at 4 °C, except for the collagenase digestion step at 37 °C. The glomeruli were used for isolation of RNA by the Qiagen RNA prep kit.

RNA-Seq

RNA samples isolated from cultured human podocytes were quantitatively and qualitatively analyzed using Nanodrop (for RNA purity (OD_{260}/OD_{280}), agarose gel electrophoresis (for RNA integrity and potential contamination), and Agilent 2100 (check RNA integrity again) by the Novogene Genome

Table 2
Primer sets used for RT-PCR

Gene	Forward primer	Reverse primer
Ift88	TGGCCAACGACCTGGAGATTAACA	ATAGCTGCTGGCTTGGGCAAATTC
Exoc1	TCTGGCAGTCAAACAGCAAC	CTTGGCATATCGGAGCAAAT
Exoc2	TACCATGGACGAAGGTCACA	CATTTTTGGCTTGTCCCACT
Exoc3	TCAAAGACATCCAGCAGTCG	GGGTCTCCCTCACAATCTCA
Exoc4	CTGGACTTTGCAAGGCAGTA	CTCCAGCTCCGTGTACTTCA
Exoc5	TGTCACCTTGGAGACCAGTTGGAAGG	GGTAACTCCTGGGCAATCAGATGC
Exoc6	GGGAAAGTTGCTCAGACAGC	CAGAGCTGGCAAACAATTCA
Exoc7	CATGGGTTATCAGGGGATTG	GAGGTCCAGGTGTGGGTAGA
Exoc8	CTG CTT GAG AAG GTG GAA GG	GGTAGCCACCAACAAGCAAT
ActB	CTTCTTGGGTATGGAATCCTGTGG	TGTGTTGGCATAGAGGTCTTTACG

Sequencing Co. Briefly, library construction was done using mRNA purified from human podocytes by poly(T) oligo-attached magnetic beads. The mRNA was fragmented randomly by addition of fragmentation buffer, and the library was prepared. After selecting the appropriate library, quality assessment was performed, and we quantified the effective concentration (>2 nM). Libraries were fed into HiSeq/MiSeq Illumina machines for RNA-Seq using a standard method by the Novogene Genome Sequencing Co. Bioinformatics and the downstream analysis was also performed by Novogene Genome Sequencing using a combination of programs, including Bowtie2, Tophat2, HTseq, Cufflink, and the wrapped scripts at Novagen. Briefly, the reference genome and gene model annotation files were obtained from the NCBI/UCSC/Ensemble genome browser. Indexes of the reference genome were built using Bowtie version 2.0.6 and paired-end clean reads were aligned to the reference genome using TopHat version 2.0.9. Quantification of the gene expression level was analyzed using HTSeq version 0.6.1, and read numbers counts were mapped for each gene. Reads per kilobase of exon model (RPKM) of each gene were calculated based on the length of the gene, and gene expression levels were analyzed. Differential expression analysis was performed using the DESeq2 R package (2_1.6.3). DESeq2 provided statistical routines for determining differential expression in digital gene expression data using a model based on the negative binomial distribution. The resulting p values were adjusted using the Benjamini and Hochberg's approach, and adjusted p values <0.05 found by DESeq2 were assigned as differentially expressed. Differential expression analysis of two conditions was performed using the DEGSeq R package (1.12.0). The p values were also adjusted using Benjamini and Hochberg method. Corrected p values of 0.005 and log2(fold change) of 1 were set as the threshold for determining significant differential expression. Correlations were determined using the corr.test function in *R* with options set alternative = "greater" and method = "Spearman." To identify the correlation between the differences, we clustered different samples using expression level RPKM with hierarchical clustering and generation of a heat map. Self-organization mapping and k means using the silhouette coefficient to adapt the optimal classification with default parameter in *R*. Gene ontology (GO) and KEGG enrichment analyses of the differentially expressed genes were analyzed using the GOseq R package. GO terms with a corrected p value less than 0.05 were considered significant. KOBAS software was used to test the statistical enrichment of differential expression genes in KEGG pathways.

Quantitative real-time RT-PCR

To evaluate the Exoc5 and Ift88 expression levels in Exoc5 and Ift88 KO mice, quantitative real-time RT-PCR (qRT-PCR) was done. Additionally, the expression of exocyst components (Exoc1–8) in Exoc5 knockdown cultured podocytes was evaluated by qRT-PCR. The specific primers were designed using Gene runner. The sequences of primers used is listed in Table 2. Quantitative RT-PCR experiments were performed using an CFX96 real-time thermal cycler (Bio-Rad) equipment and a SYBR Green PCR master mix (Bio-Rad). The thermocycling conditions utilized were s follows: an initial step of 95 °C for 3 min, 40 cycles of 95 °C for 10 s, and 60 °C for 30 s. The specificity of the amplified products was evaluated by analysis of dissociation curves generated by the equipment. Three independent RNA samples were used for analysis. The gene encoding actin protein was used as the calibrator gene. Determination of the expression ratios was performed using the threshold cycle ($\Delta\Delta C_T$) method.

Immunofluorescence microscopy and immunohistochemistry

Cells were transiently transfected with vectors using the Lipofectamine 2000 transfection agent following the manufacturer's instructions. The cells were selected for stable knockdown using puromycin. Twenty four hours post-plating and staining, the images were taken using confocal microscopy. Images of the cells were taken using a confocal microscope (Leica). Immunofluorescence staining was performed on 4-μm frozen sections from mice, and cultured podocytes were grown on coverslips as described previously (42). Each experiment was carried out in three independent sets, and the images were collected on a Leica confocal microscope (Leica TCS SP5).

Live-cell microscopy for evaluating the movement of Neph1-containing vesicles in Exoc5 knockdown cultured podocytes

mCherry–Neph1-expressing cultured podocytes, with and without Exoc5 KD, were plated on 35-mm glass-bottom cell culture plates, and the movement of Neph1-containing vesicles was analyzed using live-imaging microscopy. Images were captured for 2 min with 10-s intervals using Leica confocal microscopy (Leica TCS SP5), and images were analyzed using ImageJ software. The displacement of Neph1-containing vesicles was plotted against time. Each experiment was repeated at least three times. In each experiment, 2 million cells were plated on each coverslip, and 10 or more cells were analyzed for quantification.

Apoptosis/TUNEL assay

Frozen sections from kidneys of WT and Exoc5 knockout mutants were stained using an *in situ* cell death detection kit, fluorescein (Sigma), according to the manufacturer's instructions. The *in situ* Cell Death Detection protocol is based on the detection of single-strand DNA and dsDNA breaks (TUNEL technology: TdT-mediated dUTP-X nick end-labeling) that occur at the early stages of apoptosis.

Kidney sections were fixed and permeabilized. Subsequently, the kidney sections were incubated with the TUNEL reaction mixture that contains TdT and fluorescein dUTP. Images of the apoptotic cells in kidney sections were photographed using a confocal microscopy (Leica TCS SP5).

Animal study approval

All animal studies were conducted as per the protocols approved by the Medical University of South Carolina and/or the Ralph H. Johnson VAMC, Institutional Animal Care and Use Committee, and National Institutes of Health guidelines for the Care and Use of Laboratory Animals. Treatment of mice, including housing, injections, and surgery was in accordance with the institutional guidelines. Isoflurane anesthesia (5% induction, 2% maintenance) was used to perform all nonsurvival surgeries.

Human study approval

The CNV analysis was approved by the IRB of the University of Michigan and NEPTUNE. The human samples were deidentified.

Statistics

Each data set was presented as mean ± S.E. Statistical analysis, paired one-tailed Student's *t* test, and one-way analysis of variance was performed using the GraphPad Prism 7 software. A p value of ≤ 0.05 was considered as statistically significant.

Author contributions—D. N., A. K. S., B. R., and M. G. S. data curation; D. N., A. K. S., P. S., D. F., and C. E. G. formal analysis; D. N., E. A., M. G. S., and J. H. L. supervision; D. N., A. K. S., and J. H. L. funding acquisition; D. N., A. K. S., E. A., and B. F. investigation; D. N., A. K. S., and Y. D. methodology; D. N., A. K. S., and J. H. L. writing-original draft; D. N. and A. K. S. project administration; D. N., A. K. S., M. G. S., and J. H. L. writing-review and editing; A. K. S. validation; A. K. S. visualization; X. Z. conceptualization.

Acknowledgments—The UAB P30 Hepatorenal Fibrocystic Disease Core Center (supported by National Institutes of Health Grant P30DK074038) is gratefully acknowledged for generating the Exoc5fl/fl mouse line. The Nephrotic Syndrome Study Network Consortium (NEPTUNE, supported by Grant U54-DK-083912) is a part of the National Center for Advancing Translational Sciences (NCATS) Rare Disease Clinical Research Network (RDCRN) and is supported through a collaboration between the Office of Rare Diseases Research (ORDR), NCATS, and the NIDDK. The RDCRN is an initiative of ORDR and NCATS. Additional funding and/or programmatic support for this project has also been provided by the University of Michigan, NephCure Kidney International, and the Halpin Foundation.

References

1. Faul, C., Asanuma, K., Yanagida-Asanuma, E., Kim, K., and Mundel, P. (2007) Actin up: regulation of podocyte structure and function by components of the actin cytoskeleton. *Trends Cell Biol.* **17,** 428–437 CrossRef Medline
2. Garg, P., Verma, R., Nihalani, D., Johnstone, D. B., and Holzman, L. B. (2007) Neph1 cooperates with nephrin to transduce a signal that induces actin polymerization. *Mol. Cell. Biol.* **27,** 8698–8712 CrossRef Medline
3. Verma, R., Kovari, I., Soofi, A., Nihalani, D., Patrie, K., and Holzman, L. B. (2006) Nephrin ectodomain engagement results in Src kinase activation, nephrin phosphorylation, Nck recruitment, and actin polymerization. *J. Clin. Invest.* **116,** 1346–1359 CrossRef Medline
4. Hulkko, J., Patrakka, J., Lal, M., Tryggvason, K., Hultenby, K., and Wernerson, A. (2014) Neph1 is reduced in primary focal segmental glomerulosclerosis, minimal change nephrotic syndrome, and corresponding experimental animal models of adriamycin-induced nephropathy and puromycin aminonucleoside nephrosis. *Nephron Extra* **4,** 146–154 CrossRef Medline
5. Wagner, M. C., Rhodes, G., Wang, E., Pruthi, V., Arif, E., Saleem, M. A., Wean, S. E., Garg, P., Verma, R., Holzman, L. B., Gattone, V., Molitoris, B. A., and Nihalani, D. (2008) Ischemic injury to kidney induces glomerular podocyte effacement and dissociation of slit diaphragm proteins Neph1 and ZO-1. *J. Biol. Chem.* **283,** 35579–35589 CrossRef Medline
6. Swiatecka-Urban, A. (2017) Endocytic trafficking at the mature podocyte slit diaphragm. *Front. Pediatr.* **5,** 32 CrossRef Medline
7. Lipschutz, J. H., and Mostov, K. E. (2002) Exocytosis: the many masters of the exocyst. *Curr. Biol.* **12,** R212–R214 CrossRef Medline
8. Grindstaff, K. K., Yeaman, C., Anandasabapathy, N., Hsu, S. C., Rodriguez-Boulan, E., Scheller, R. H., and Nelson, W. J. (1998) Sec6/8 complex is recruited to cell-cell contacts and specifies transport vesicle delivery to the basal-lateral membrane in epithelial cells. *Cell* **93,** 731–740 CrossRef Medline
9. Lipschutz, J. H., Guo, W., O'Brien, L. E., Nguyen, Y. H., Novick, P., and Mostov, K. E. (2000) Exocyst is involved in cystogenesis and tubulogenesis and acts by modulating synthesis and delivery of basolateral plasma membrane and secretory proteins. *Mol. Biol. Cell* **11,** 4259–4275 CrossRef Medline
10. Fogelgren, B., Lin, S. Y., Zuo, X., Jaffe, K. M., Park, K. M., Reichert, R. J., Bell, P. D., Burdine, R. D., and Lipschutz, J. H. (2011) The exocyst protein Sec10 interacts with polycystin-2 and knockdown causes PKD-phenotypes. *PLoS Genet.* **7,** e1001361 CrossRef Medline
11. Seixas, C., Choi, S. Y., Polgar, N., Umberger, N. L., East, M. P., Zuo, X., Moreiras, H., Ghossoub, R., Benmerah, A., Kahn, R. A., Fogelgren, B., Caspary, T., Lipschutz, J. H., and Barral, D. C. (2016) Arl13b and the exocyst interact synergistically in ciliogenesis. *Mol. Biol. Cell* **27,** 308–320 CrossRef Medline
12. Zuo, X., Fogelgren, B., and Lipschutz, J. H. (2011) The small GTPase Cdc42 is necessary for primary ciliogenesis in renal tubular epithelial cells. *J. Biol. Chem.* **286,** 22469–22477 CrossRef Medline
13. Zuo, X., Guo, W., and Lipschutz, J. H. (2009) The exocyst protein Sec10 is necessary for primary ciliogenesis and cystogenesis *in vitro*. *Mol. Biol. Cell* **20,** 2522–2529 CrossRef Medline
14. Lipschutz, J. H., Lingappa, V. R., and Mostov, K. E. (2003) The exocyst affects protein synthesis by acting on the translocation machinery of the endoplasmic reticulum. *J. Biol. Chem.* **278,** 20954–20960 CrossRef Medline
15. Toikkanen, J. H., Miller, K. J., Söderlund, H., Jäntti, J., and Keränen, S. (2003) The β subunit of the Sec61p ER translocon interacts with the exocyst complex in *Saccharomyces cerevisiae*. *J. Biol. Chem.* **278,** 20946–20953 CrossRef Medline
16. Lobo, G. P., Fulmer, D., Guo, L., Zuo, X., Dang, Y., Kim, S. H., Su, Y., George, K., Obert, E., Fogelgren, B., Nihalani, D., Norris, R. A., Rohrer, B., and Lipschutz, J. H. (2017) The exocyst is required for photoreceptor ciliogenesis and retinal development. *J. Biol. Chem.* **292,** 14814–14826 CrossRef Medline
17. Dixon-Salazar, T. J., Silhavy, J. L., Udpa, N., Schroth, J., Bielas, S., Schaffer, A. E., Olvera, J., Bafna, V., Zaki, M. S., Abdel-Salam, G. H., Mansour, L. A.,

Selim, L., Abdel-Hadi, S., Marzouki, N., Ben-Omran, T., *et al.* (2012) Exome sequencing can improve diagnosis and alter patient management. *Sci. Transl. Med.* **4,** 138ra78 CrossRef Medline

18. Verbitsky, M., Sanna-Cherchi, S., Fasel, D. A., Levy, B., Kiryluk, K., Wuttke, M., Abraham, A. G., Kaskel, F., Köttgen, A., Warady, B. A., Furth, S. L., Wong, C. S., and Gharavi, A. G. (2015) Genomic imbalances in pediatric patients with chronic kidney disease. *J. Clin. Invest.* **125,** 2171–2178 CrossRef Medline
19. Sanna-Cherchi, S., Kiryluk, K., Burgess, K. E., Bodria, M., Sampson, M. G., Hadley, D., Nees, S. N., Verbitsky, M., Perry, B. J., Sterken, R., Lozanovski, V. J., Materna-Kiryluk, A., Barlassina, C., Kini, A., Corbani, V., *et al.* (2012) Copy-number disorders are a common cause of congenital kidney malformations. *Am. J. Hum. Genet.* **91,** 987–997 CrossRef Medline
20. Gadegbeku, C. A., Gipson, D. S., Holzman, L. B., Ojo, A. O., Song, P. X., Barisoni, L., Sampson, M. G., Kopp, J. B., Lemley, K. V., Nelson, P. J., Lienczewski, C. C., Adler, S. G., Appel, G. B., Cattran, D. C., Choi, M. J., *et al.* (2013) Design of the Nephrotic Syndrome Study Network (NEPTUNE) to evaluate primary glomerular nephropathy by a multidisciplinary approach. *Kidney Int.* **83,** 749–756 CrossRef Medline
21. Mei, K., Li, Y., Wang, S., Shao, G., Wang, J., Ding, Y., Luo, G., Yue, P., Liu, J. J., Wang, X., Dong, M. Q., Wang, H. W., and Guo, W. (2018) Cryo-EM structure of the exocyst complex. *Nat. Struct. Mol. Biol.* **25,** 139–146 CrossRef Medline
22. Picco, A., Irastorza-Azcarate, I., Specht, T., Böke, D., Pazos, I., Rivier-Cordey, A. S., Devos, D. P., Kaksonen, M., and Gallego, O. (2017) The *in vivo* architecture of the exocyst provides structural basis for exocytosis. *Cell* **168,** 400–412.e18 CrossRef Medline
23. Choi, S. Y., Chacon-Heszele, M. F., Huang, L., McKenna, S., Wilson, F. P., Zuo, X., and Lipschutz, J. H. (2013) Cdc42 deficiency causes ciliary abnormalities and cystic kidneys. *J. Am. Soc. Nephrol.* **24,** 1435–1450 CrossRef Medline
24. Zhang, X., Bi, E., Novick, P., Du, L., Kozminski, K. G., Lipschutz, J. H., and Guo, W. (2001) Cdc42 interacts with the exocyst and regulates polarized secretion. *J. Biol. Chem.* **276,** 46745–46750 CrossRef Medline
25. Fogelgren, B., Polgar, N., Lui, V. H., Lee, A. J., Tamashiro, K. K., Napoli, J. A., Walton, C. B., Zuo, X., and Lipschutz, J. H. (2015) Urothelial defects from targeted inactivation of exocyst Sec10 in mice cause ureteropelvic junction obstructions. *PLoS ONE* **10,** e0129346 CrossRef Medline
26. Arif, E., Solanki, A. K., Srivastava, P., Rahman, B., Tash, B. R., Holzman, L. B., Janech, M. G., Martin, R., Knölker, H.-J., Fitzgibbon, W. R., Deng, P., Budisavljevic, M. N., Syn, W.-K., Wang, C., Lipschutz, J. H., *et al.* (2019) The motor protein Myo1c regulates transforming growth factor-β-signaling and fibrosis in podocytes. *Kidney Int.* **95,** CrossRef
27. Tryggvason, K., Patrakka, J., and Wartiovaara, J. (2006) Hereditary proteinuria syndromes and mechanisms of proteinuria. *N. Engl. J. Med.* **354,** 1387–1401 CrossRef Medline
28. Assady, S., Wanner, N., Skorecki, K. L., and Huber, T. B. (2017) New insights into podocyte biology in glomerular health and disease. *J. Am. Soc. Nephrol.* **28,** 1707–1715 CrossRef Medline
29. Perico, L., Conti, S., Benigni, A., and Remuzzi, G. (2016) Podocyte-actin dynamics in health and disease. *Nat. Rev. Nephrol.* **12,** 692–710 CrossRef Medline
30. Takei, R., Katoh, Y., and Nakayama, K. (2018) Robust interaction of IFT70 with IFT52–IFT88 in the IFT-B complex is required for ciliogenesis. *Biol. Open* **7,** bio033241 CrossRef Medline
31. Yoder, B. K. (2007) Role of primary cilia in the pathogenesis of polycystic kidney disease. *J. Am. Soc. Nephrol.* **18,** 1381–1388 CrossRef Medline
32. Yoder, B. K., Richards, W. G., Sweeney, W. E., Wilkinson, J. E., Avener, E. D., and Woychik, R. P. (1995) Insertional mutagenesis and molecular analysis of a new gene associated with polycystic kidney disease. *Proc. Assoc. Am. Physicians* **107,** 314–323 Medline
33. Grahammer, F., Wigge, C., Schell, C., Kretz, O., Patrakka, J., Schneider, S., Klose, M., Kind, J., Arnold, S. J., Habermann, A., Bräuniger, R., Rinschen, M. M., Völker, L., Bregenzer, A., Rubbenstroth, D., *et al.* (2016) A flexible, multilayered protein scaffold maintains the slit in between glomerular podocytes. *JCI Insight* **1,** 86177 CrossRef Medline
34. Özkan, E., Chia, P. H., Wang, R. R., Goriatcheva, N., Borek, D., Otwinowski, Z., Walz, T., Shen, K., and Garcia, K. C. (2014) Extracellular architecture of the SYG-1/SYG-2 adhesion complex instructs synaptogenesis. *Cell* **156,** 482–494 CrossRef Medline
35. Sagar, A., Arif, E., Solanki, A. K., Srivastava, P., Janech, M. G., Kim, S. H., Lipschutz, J. H., Kwon, S. H., Ashish, and Nihalani, D. (2017) Targeting Neph1 and ZO-1 protein–protein interaction in podocytes prevents podocyte injury and preserves glomerular filtration function. *Sci. Rep.* **7,** 12047 CrossRef Medline
36. Agrawal, S., Guess, A. J., Chanley, M. A., and Smoyer, W. E. (2014) Albumin-induced podocyte injury and protection are associated with regulation of COX-2. *Kidney Int.* **86,** 1150–1160 CrossRef Medline
37. Robins, R., Baldwin, C., Aoudjit, L., Gupta, I. R., and Takano, T. (2015) Loss of Rho-GDIα sensitizes podocytes to lipopolysaccharide-mediated injury. *Am. J. Physiol. Renal Physiol.* **308,** F1207–F1216 CrossRef Medline
38. Mundel, P., and Reiser, J. (2010) Proteinuria: an enzymatic disease of the podocyte? *Kidney Int.* **77,** 571–580 CrossRef Medline
39. Lennon, J. C., Butini, S., Campiani, G., O'Meara, A., Williams, D. C., and Zisterer, D. M. (2016) Involvement of AMP-activated protein kinase in mediating pyrrolo-1,5-benzoxazepine-induced apoptosis in neuroblastoma cells. *Invest. New Drugs* **34,** 663–676 CrossRef Medline
40. Kim, J., Lee, J. E., Heynen-Genel, S., Suyama, E., Ono, K., Lee, K., Ideker, T., Aza-Blanc, P., and Gleeson, J. G. (2010) Functional genomic screen for modulators of ciliogenesis and cilium length. *Nature* **464,** 1048–1051 CrossRef Medline
41. Velez, J. C. Q., Arif, E., Rodgers, J., Hicks, M. P., Arthur, J. M., Nihalani, D., Bruner, E. T., Budisavljevic, M. N., Atkinson, C., Fitzgibbon, W. R., and Janech, M. G. (2017) Deficiency of the angiotensinase aminopeptidase a increases susceptibility to glomerular injury. *J. Am. Soc. Nephrol.* **28,** 2119–2132 CrossRef Medline
42. Arif, E., Rathore, Y. S., Kumari, B., Ashish, F., Wong, H. N., Holzman, L. B., and Nihalani, D. (2014) Slit diaphragm protein Neph1 and its signaling: a novel therapeutic target for protection of podocytes against glomerular injury. *J. Biol. Chem.* **289,** 9502–9518 CrossRef Medline
43. Hattori, S., Kanda, S., and Harita, Y. (2011) Tyrosine kinase signaling in kidney glomerular podocytes. *J. Signal. Transduct.* **2011,** 317852 CrossRef Medline
44. Akhurst, R. J., and Hata, A. (2012) Targeting the TGFβ signalling pathway in disease. *Nat. Rev. Drug Discov.* **11,** 790–811 CrossRef Medline
45. Herman-Edelstein, M., Weinstein, T., and Gafter, U. (2013) TGFβ1-dependent podocyte dysfunction. *Curr. Opin. Nephrol. Hypertens.* **22,** 93–99 CrossRef Medline
46. Kim, J. H., Kim, B. K., Moon, K. C., Hong, H. K., and Lee, H. S. (2003) Activation of the TGF-β/Smad signaling pathway in focal segmental glomerulosclerosis. *Kidney Int.* **64,** 1715–1721 CrossRef Medline
47. Blattner, S. M., Hodgin, J. B., Nishio, M., Wylie, S. A., Saha, J., Soofi, A. A., Vining, C., Randolph, A., Herbach, N., Wanke, R., Atkins, K. B., Gyung Kang, H., Henger, A., Brakebusch, C., Holzman, L. B., and Kretzler, M. (2013) Divergent functions of the Rho GTPases Rac1 and Cdc42 in podocyte injury. *Kidney Int.* **84,** 920–930 CrossRef Medline
48. 1000 Genomes Project Consortium, Auton, A., Brooks, L. D., Durbin, R. M., Garrison, E. P., Kang, H. M., Korbel, J. O., Marchini, J. L., McCarthy, S., McVean, G. A., and Abecasis, G. R. (2015) A global reference for human genetic variation. *Nature* **526,** 68–74 CrossRef Medline
49. George, B., and Holzman, L. B. (2012) Signaling from the podocyte intercellular junction to the actin cytoskeleton. *Semin. Nephrol.* **32,** 307–318 CrossRef Medline
50. Johnstone, D. B., Zhang, J., George, B., Léon, C., Gachet, C., Wong, H., Parekh, R., and Holzman, L. B. (2011) Podocyte-specific deletion of Myh9 encoding nonmuscle myosin heavy chain 2A predisposes mice to glomerulopathy. *Mol. Cell. Biol.* **31,** 2162–2170 CrossRef Medline
51. Arif, E., Wagner, M. C., Johnstone, D. B., Wong, H. N., George, B., Pruthi, P. A., Lazzara, M. J., and Nihalani, D. (2011) Motor protein Myo1c is a podocyte protein that facilitates the transport of slit diaphragm protein Neph1 to the podocyte membrane. *Mol. Cell. Biol.* **31,** 2134–2150 CrossRef Medline
52. Saleem, M. A., O'Hare, M. J., Reiser, J., Coward, R. J., Inward, C. D., Farren, T., Xing, C. Y., Ni, L., Mathieson, P. W., and Mundel, P. (2002) A conditionally immortalized human podocyte cell line demonstrating nephrin and podocin expression. *J. Am. Soc. Nephrol.* **13,** 630–638 Medline

53. Srivastava P, Solanki A. K., Arif E., Wolf B. J., Janech M. G., Budisavljevic M. N., Sang-Ho Kwon S.-H., Nihalani D. (2019) Development of a novel cell-based assay to diagnose recurrent focal segmental glomerulosclerosis patients. *Kidney Int.* **95,** 708–716 CrossRef Medline
54. Solanki, A. K., Arif, E., Morinelli, T., Wilson, R. C., Hardiman, G., Deng, P., Arthur, J. M., Velez, J. C., Nihalani, D., Janech, M. G., and Budisavljevic, M. N. (2018) A novel CLCN5 mutation associated with focal segmental glomerulosclerosis and podocyte injury. *Kidney Int. Rep.* **3,** 1443–1453 CrossRef Medline
55. Arif, E., Sharma, P., Solanki, A., Mallik, L., Rathore, Y. S., Twal, W. O., Nath, S. K., Gandhi, D., Holzman, L. B., Ostap, E. M., Ashish, and Nihalani, D. (2016) Structural analysis of the Myo1c and Neph1 complex provides insight into the intracellular movement of Neph1. *Mol. Cell. Biol.* **36,** 1639–1654 CrossRef Medline